Available online at www.sciencedirect.com
SCIENCE DIRECT®
Journal of Solid State Chemistry 178 (2005) 2390–2393
JOURNAL OF SOLID STATE CHEMISTRY
www.elsevier.com/locate/jssc

Rapid communication

Magnetic iron nitride nanodendrites

Minhua Cao[a,*], Tianfu Liu[b], Genban Sun[b], Xinglong Wu[a], Xiaoyan He[a], Changwen Hu[a,b]

[a]*Institute of Polyoxometalate Chemistry, Northeast Normal University, Changchun 130024, PR China*
[b]*Department of Chemistry, Beijing Institute of Technology, Beijing 100081, PR China*

Received 28 March 2005; received in revised form 24 April 2005; accepted 30 April 2005
Available online 1 June 2005

Abstract

We report the synthesis of Fe_3N nanodendrites directly by reduction-nitriding of α-Fe_2O_3 nanopine dendrites in a mixed stream of H_2–NH_3. Fe_3N basically retains dendritic morphology of the starting material α-Fe_2O_3. It is found that nanorod branches of Fe_3N dendrites have relatively uniform diameters and are evenly distributed at both sides of the stem with a periodicity of about 50 nm. The diameters of the nanorods are about 50 nm, and their lengths range from 50 to 1000 nm. Fe_3N nanodendrites show a rapid saturation of magnetization of 104 emu/g at 300 K, as expected for a magnet.

Keywords: Iron nitride; Nanodendrites; Magnetic; Nitridation

In recent years, anisotropic growth of nanomaterials have generated a wide variety of nanostructures, including tubes/wires/rods [1,2], cubes [3,4], nanodisks [5], dendrites [6], prisms [7], tetrapods [8] and so on, and some of them have been shown to display unique physical properties. It is generally believed that intrinsic properties of a nanostructure are mainly determined by its size, shape, composition, crystallinity, and crystal structure, in which the shape is thought to be one of the most important factors. Especially for a magnetic nanostructure, controlling its shape is of crucial importance as shape may lead to anisotropic magnetic properties of a nanomaterial, which are necessary for magnetic nanomaterials to be ferromagnetic at room temperature. Iron nitrides (FeN_x) have attracted intensive attention due to their diverse structures and potentially technological applications. In particular, those with small N contents have been investigated as materials for advanced magnetic data storage applications [9]. In this respect, nanoscale iron nitrides with anisotropic growth may offer greater potential as building blocks for applications in nanodevices. However, very few studies on their synthesis and magnetic properties have been reported to date [9–12]. Among several reported synthesis methods, reduction-nitriding is a simple and convenient method to synthesize iron nitrides [9]. Recently, our group has successfully synthesized magnetic α-Fe_2O_3 nanopine dendrites using a hydrothermal method [13], therefore, it is necessary to further treat the resulting α-Fe_2O_3 nanopine dendrites to obtain the desirable products and morphologies. In this letter, we report the fabrication of magnetic iron nitride nanodendrites by dealing with the as-synthesized α-Fe_2O_3 nanopine dendrites under a mixed stream of H_2–NH_3. By precisely controlling the reduction-nitriding temperature and the volume ratio of H_2 to NH_3, we were able to synthesize Fe_3N with dendritic morphology and Fe_4N with conglomeration, respectively.

The starting material α-Fe_2O_3 nanopine dendrites were synthesized under hydrothermal conditions at 140 °C [12]. In a typical synthesis of iron nitrides, α-Fe_2O_3 powers were loaded into a quartz tube, which was centered into a horizontal tube furnace, through which a H_2/NH_3 mixture with the volume ratio of 1:2 was passed, and the reaction was kept at 500 °C for 4 h. After the reduction-nitriding process was finished, black Fe_3N powder was formed. When the H_2/NH_3 mixture with the

*Corresponding author. Fax: +86 431 566 3503.
E-mail address: caomh043@nenu.edu.cn (M. Cao).

0022-4596/$ - see front matter © 2005 Elsevier Inc. All rights reserved.
doi:10.1016/j.jssc.2005.04.035

volume ratio of 1:1 was used and the reaction was kept at 600 °C for 4 h, Fe_4N was obtained. The compositional analysis of samples was examined using an X-ray diffractometer with Cu$K\alpha$ radiation. The morphology and microstructure of samples were obtained by scanning electron microscopy (SEM), transmission electron microscopy (TEM), selected area electron diffraction (SAED), and high-resolution TEM (HRTEM). The magnetization data of the samples were collected over the temperature range of 5–300 K using a Quantum Design MPMS-5S super-conducting quantum interference device (SQUID) magnetometer.

Fig. 1 shows the X-ray diffraction patterns of the samples obtained under the above two reaction conditions. The strong diffraction peaks in Fig. 1b can be indexed to hexagonal Fe_3N with lattice constants $a = 2.695$ Å and $c = 4.362$ Å (JCPDS 01-1236), while those in Fig. 1c can be indexed to the cubic Fe_4N with lattice constant $a = 3.790$ Å (JCPDS 8-19); these results are consistent with those of Fe_3N and Fe_4N bulk crystals [14], respectively. In addition, there existed several very weak peaks in XRD images, which can be indexed to the α-Fe_2O_3. This is due to the incomplete reduction-nitriding of the starting material α-Fe_2O_3 resulting from the inexact apparatus used. If a precision apparatus can be available, pure iron nitride would be obtained.

Fig. 2 shows the SEM and TEM images of the starting material α-Fe_2O_3 nanopine dendrites prepared by simple hydrothermal method. The low magnification image in Fig. 2 shows that the starting material consists almost entirely of dendritic structures. A single dendrite shown in Fig. 2b and c displays an evident fractal structure characteristic, with an outstanding stem and highly ordered branches distributed at both sides of the stem. Similarly, each branch of the dendrite also displays such structural characteristic.

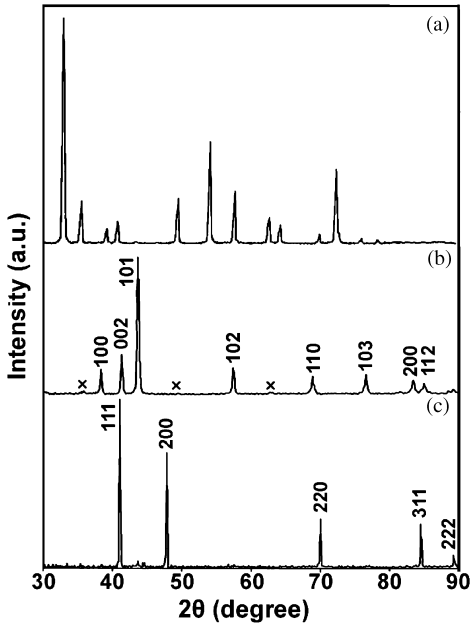

Fig. 1. XRD images of α-Fe_2O_3 nanopine dendrites (a), Fe_3N nanodendrites (b), and Fe_4N particles (c).

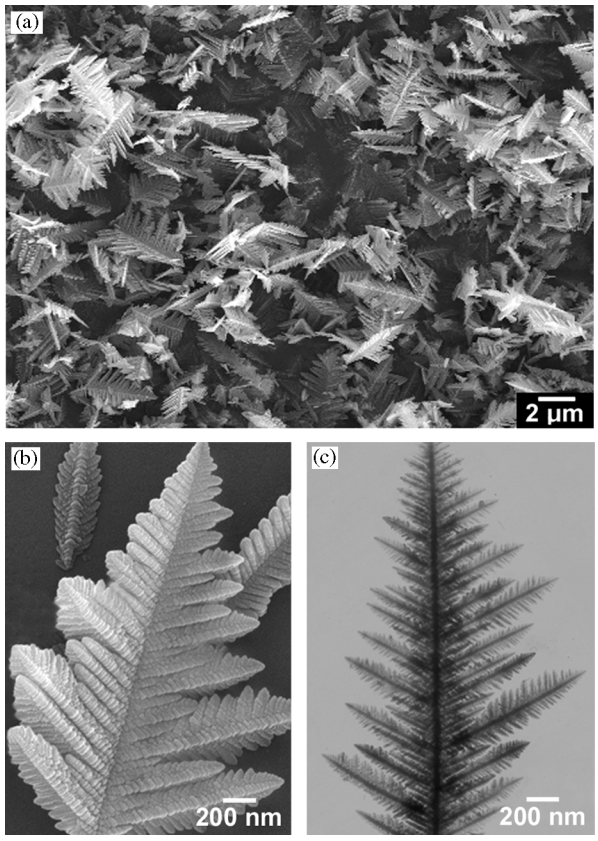

Fig. 2. (a) SEM image of α-Fe_2O_3 nanopine dendrites. (b) SEM image of a single α-Fe_2O_3 nanopine dendrite. (c) TEM image of a single α-Fe_2O_3 nanopine dendrite.

When the starting material α-Fe_2O_3 nanopine dendrites were treated by a reduction-nitriding process at 500 °C, Fe_3N was obtained, which has been determined by XRD image. Fig. 3a shows the low magnification TEM image of Fe_3N sample. It is evident that the product is dominated by dendritic structures. The high magnification in Fig. 3b shows the morphology of a single dendrite. It can be found that the morphology of Fe_3N, compared to that of the starting material α-Fe_2O_3, changes largely, and an evident transition from hyperbranched dendrites for α-Fe_2O_3 to nanorod branched dendrites for Fe_3N is observed, which may result from the high-temperature treatment. In this process, Fe_3N basically retains the dendritic morphology of the starting material but without fractal structure characteristic. It can be seen from the TEM image that nanorod branches of Fe_3N dendrites have relatively uniform diameters and are evenly distributed at both sides of the stem with a periodicity of about 50 nm. The

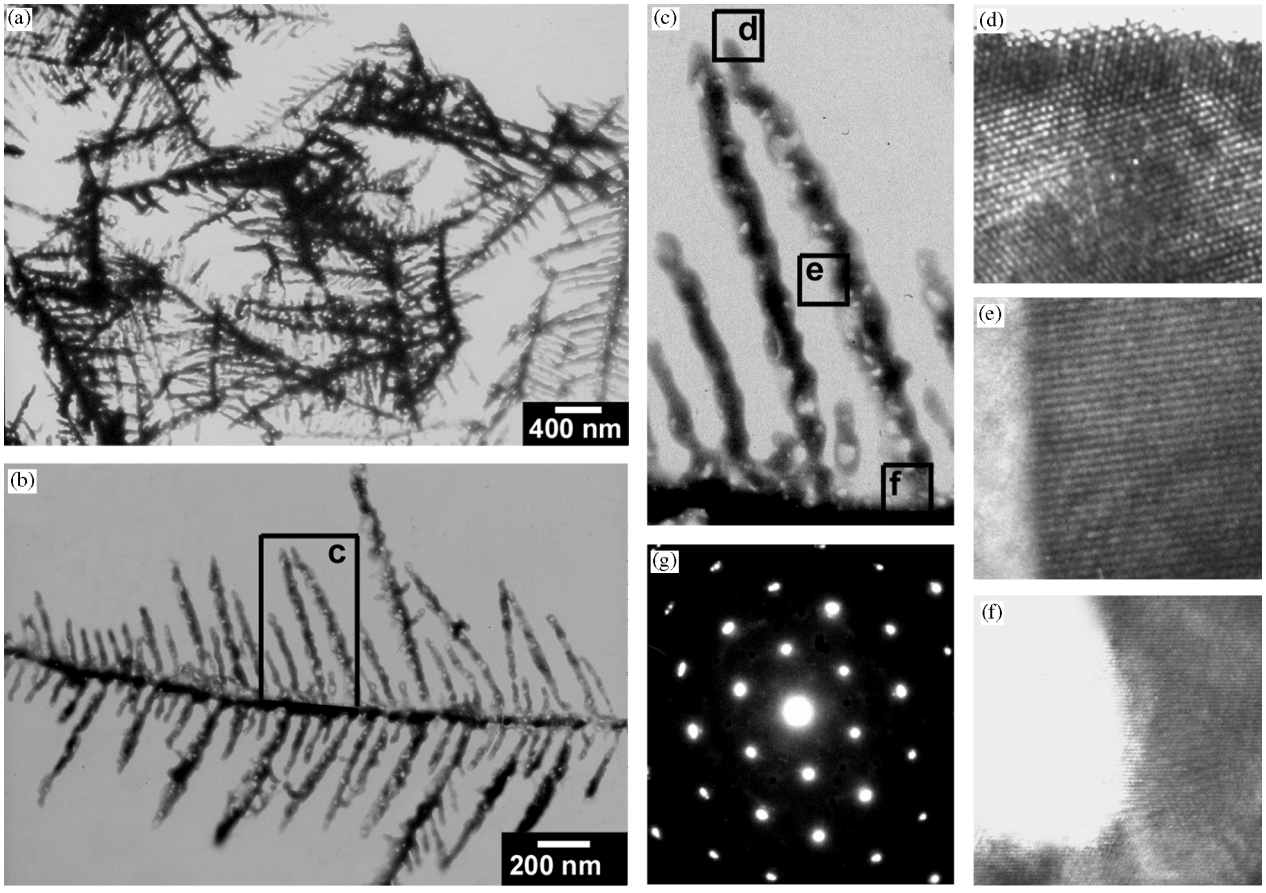

Fig. 3. (a) Low magnification TEM image of Fe_3N nanodendrites. (b) TEM image of a single Fe_3N nanodendrite. (c) Enlarged nanodendrite recorded in (b). (d–f) HRTEM images recorded in different regions of the dendritic structure in (c). (g) SAED image recorded on the entire dendritic structure in (b).

diameters of the nanorods are about 50 nm, and their lengths range from 50 to 1000 nm. The microstructure of the dendrites was further examined by HRTEM and SAED. Fig. 3d–f shows HRTEM images taken in different areas on a single dendrite as shown in Fig. 3c. It is clear that all of them show clear lattice fringes, indicating the single-crystalline nature of the whole dendrite. The lattice spacing of 2.089 Å between adjacent lattice planes in each of these images corresponds to the distance between two (101) crystal planes, indicating that both the stem and all branches of Fe_3N dendrite is oriented in [101] direction. The SAED taken on the same dendrite but at different areas all shown the same image as shown in Fig. 3g, also confirming the single-crystalline nature of the dendrite.

When the starting material α-Fe_2O_3 nanopine dendrites were treated at 600 °C, Fe_4N was formed as confirmed by XRD image. The reduction-nitriding temperature had to be higher than 600 °C, otherwise impurity product was obtained. The TEM image of Fe_4N samples is shown in Fig. 4. It is clear that the samples were large irregular aggregates of roughly spherical particles instead of dendrites. The reason

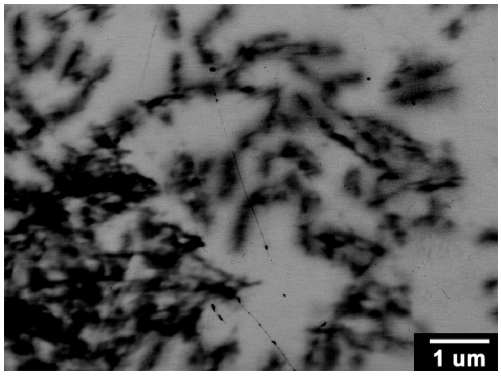

Fig. 4. TEM image of Fe_4N particles.

may be that α-Fe_2O_3 nanopine dendrites partly sintered in the process of high-temperature reactions, resulting in the agglomeration of the product.

The field dependence of the magnetization (0–50 kOe) for Fe_3N nanodendrites measured at 300 K (Fig. 5), shows a rapid saturation of magnetization, as expected for a magnet. The saturation magnetization reaches a value of 104 emu/g, lower than the literature value [10].

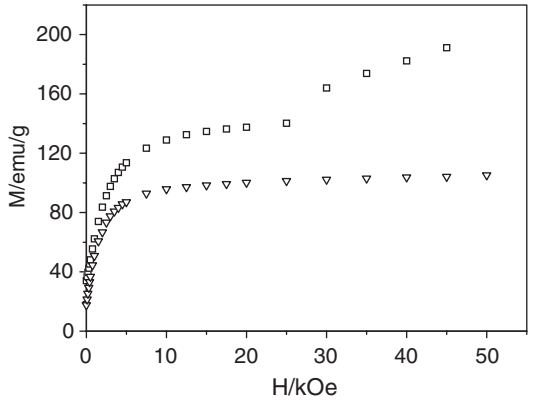

Fig. 5. Field dependence of magnetization for Fe_3N, □ at 5 K, △ at 300 K.

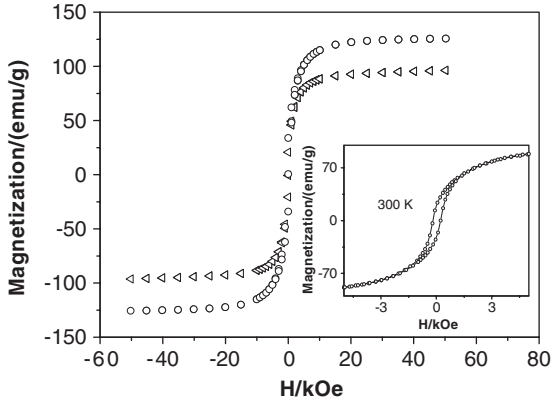

Fig. 6. Hysteresis loop curves measured on Fe_3N nanodendrites, ○ at 300 K, △ at 5 K, respectively. The inset is a blow-up in the region of −5 to 5 kOe at 300 K.

The magnetization reaches 140 emu/g before 25 kOe, then it increases rapidly to 190 emu/g at 45 kOe measured at 5 K. A hysteresis loop at 5 and 300 K (Fig. 6) for Fe_3N is observed. The coercive force and remanent magnetization of Fe_3N are 226 Oe and 19.6 emu/g, respectively, which can be clearly observed in the region of −5 to 5 kOe at 300 K (inset of Fig. 6). The existence of hysteresis loop for Fe_3N nanodendrites can be explained by the incomplete conversion from α-Fe_2O_3 to Fe_3N during the reduction-nitriding procedure. At 300 K, antiferromagnetic interaction of small residue α-Fe_2O_3 can be ignored. At low temperature (5 K), the increase of saturation magnetization may be caused by nanosize effect of small residue α-Fe_2O_3, although it has not found phase translation from antiferromagnetism to paramagnetism or superparamagnetic phenomenon [13] in pure α-Fe_2O_3 nanopine dendrites. The coercive force and saturation magnetization of the Fe_3N nanodendrites are different from those of Fe_3N nanoparticles obtained using Fe_3O_4 or γ-Fe_2O_3 as the starting materials [9,10] which indicates that magnetization of Fe_3N sample is shape-dependent.

In summary, dendritic iron nitrides have been prepared through a reduction-nitriding process by using α-Fe_2O_3 nanopine dendrites as starting material. By precisely controlling the reduction-nitriding temperature and the volume ratio of H_2 to NH_3, Fe_3N with dendritic shape and Fe_4N with conglomeration were obtained, respectively. The synthesized dendritic Fe_3N are single-crystal. Fe_3N nanodendrites have a low saturation magnetization of 104 emu/g at 300 K, whereas at low temperature (5 K), Fe_3N nanodendrites show an increase of saturation magnetization, which may be caused by nanosize effect of small residue α-Fe_2O_3.

Acknowledgment

This work was supported by the Natural Science Fund Council of China (NSFC, Nos. 20331010, 20271007, 90406002 and 20401005) and Specialized Research Fund for the Doctoral Program of Higher Education (SRFDP, No. 20030007014). This work was supported also by Jilin Distinguished Young Scholars Program and the Natural Science Young Foundation of Northeast Normal University.

References

[1] S. Iijima, Nature 354 (1991) 56.
[2] X.G. Peng, L. Manna, W.D. Yang, J. Wickham, E. Scher, A. Kadavanich, A.P. Alivisatos, Nature 404 (2000) 59.
[3] Y.G. Sun, Y.N. Xia, Science 298 (2004) 2176.
[4] F. Dumestre, B. Chaudret, C. Amiens, P. Renaud, P. Fejes, Science 303 (2004) 821.
[5] C.X. Xu, X.W. Sun, Z.L. Dong, M.B. Yu, Appl. Phys. Lett. 85 (2004) 3160.
[6] H. Yan, R. He, J. Johnson, M. Law, R.J. Saykally, P.D. Yang, J. Am. Chem. Soc. 125 (2003) 4728.
[7] R.C. Jin, Y.W. Cao, C.A. Mirkin, K.L. Kelly, G.C. Schatz, J.G. Zheng, Science 294 (2001) 1901.
[8] L.M. Manna, D.J. Milliron, A. Meisel, E.C. Scher, A.P. Alivisatos, Nat. Mater. 2 (2003) 382.
[9] D. Andriamandroso, L. Fefilatiev, G. Demazeau, L. Fournès, M. Pouchard, Mater. Res. Bull. 19 (1984) 1187.
[10] Z.Q. Yu, J.R. Zhang, Y.W. Du, J. Magn. Magn. Mater. 159 (1996) L8.
[11] X.L. Wu, W. Zhong, N.J. Tang, H.Y. Jiang, W. Liu, Y.W. Du, J. Alloys Compd. 385 (2004) 294.
[12] D. Li, C.J. Choi, J.H. Yu, B.K. Kim, Z.D. Zhang, J. Magn. Magn. Mater. 283 (2004) 8.
[13] M.H. Cao, T.F. Liu, S. Gao, G.B. Sun, C.W. Hu, Z.L. Wang, Angew. Chem. Int. Ed. (2005), in press.
[14] H. Jacobs, D. Rechenbach, U. Zachwieja, J. Alloys Compd. 227 (1995) 10.